*minerals*

MDPI

*Article*

# Genetic Mechanism of Tabular-Shaped Orebody of the Hailijin Sandstone-Type Uranium Deposit in the Songliao Basin: Constraints on the Clay Mineralogy of Ore-Bearing Sandstone

**Mingming Tian [1], Ziying Li [1,*], Yunlong Zhang [1], Licheng Jia [1], Jun Ning [2], Jimu Li [2], Hanghang He [2] and Guolong Tang [2]**

[1] Beijing Research Institute of Uranium Geology, Beijing 100029, China; tian_ming_ming@126.com (M.T.); yunlongzhangbriug@126.com (Y.Z.)
[2] No.243 Geological Party of China National Nuclear Corporation (CNNC), Chifeng 024006, China
* Correspondence: zyli9818@126.com

**Abstract:** The Hailijin (HLJ) sandstone-type uranium deposit was newly discovered in the southwestern Songliao Basin in recent years. Different from the roll-front orebody of the sandstone-type uranium deposits with (phreatic oxidation) interlayer redox origin (or phreatic oxidation), the orebody of the HLJ uranium deposit is tabular-shaped and multi-stratiform. The kaolinite content in ore-controlling gray sandstones is significantly higher than that in oxidized sandstones, which have the highest kaolinite content in the less oxidized zone of sandstone-type uranium deposits in the basins of western China (such as Yili Basin and Turpan-Hami Basin). In order to identify the properties of ore-forming fluids and the genesis of the tabular-shaped orebody of the HLJ uranium deposit, trace element, scanning electron microscopy (SEM), X-ray diffraction (XRD), and uranium mineral electron probe (EPMA) analyses of different geochemical zone sandstones in ore-bearing strata were carried out. As a result, kaolinite, illite, and illite/smectite formation (I/S) appear to alternate with one another in ore-controlling gray sandstones, and the content of kaolinite is the highest in ores. SEM analysis also suggests that uranium minerals are commonly adsorbed on the surface of foliated and vermicular kaolinite or trapped within micropores of kaolinite. In this case, it is inferred that kaolinite in ore-controlling gray sandstones is of epigenetic origin, and the ore-bearing sandstones have undergone at least one transformation of acidic fluids. Combined with the regional paleoclimate, regional tectonics, and regional burial history, it is concluded that the acidic fluid originated from the uranium-rich source rocks of the Lower Cretaceous Jiufotang Formation, and the tabular-shaped orebody of the HLJ uranium deposit was formed by exudative metallogeny. When the uranium-rich acidic organic fluids exuded upward from deep levels along the faults to the target strata, the solubility of uranium and other polymetallic elements decreased because of the decrease in temperature and pressure, and uranium eventually precipitated and accumulated in sandstones with suitable permeability and porosity. However, it cannot be ruled out that the superimposition and transformation of uranium mineralization was caused by phreatic oxidation or local interlayer redox during the interval of exudative metallogeny.

**Keywords:** clay minerals; acidic organic fluid; tabular-shaped orebody; Hailijin sandstone-type uranium deposit; Songliao Basin



**Citation:** Tian, M.; Li, Z.; Zhang, Y.; Jia, L.; Ning, J.; Li, J.; He, H.; Tang, G. Genetic Mechanism of Tabular-Shaped Orebody of the Hailijin Sandstone-Type Uranium Deposit in the Songliao Basin: Constraints on the Clay Mineralogy of Ore-Bearing Sandstone. *Minerals* **2023**, *13*, 1324. https://doi.org/10.3390/min13101324

Academic Editor: Sergey V. Krivovichev

Received: 27 August 2023
Revised: 28 September 2023
Accepted: 28 September 2023
Published: 13 October 2023



## 1. Introduction

In recent years, a series of remarkable achievements regarding uranium exploration have occurred in the southwestern Songliao Basin, and a large number of large or super-sized sandstone-type uranium deposits (such as Qianjiadian uranium deposit, Baolongshan uranium deposit, HLJ uranium deposit, and Dalin uranium deposit) have been newly discovered [1–5]. The uranium orebody is a multi-stratiform and tabular-shaped orebody [6–8],

which is obviously different from those of roll-front form orebodies in sandstone-type uranium deposits of interlayer oxidation zone origin (such as the Mengqiguer uranium deposit in the Yili Basin, the Shihongtan uranium deposit in the Turpan-Hami Basin, the Dongsheng uranium deposit in the Ordos Basin, and the Bayinwula uranium deposit in the Erlian Basin) [9–13]. In addition, normally, kaolinite is rich in ore-bearing sandstones, especially in less oxidized sandstones of interlayer oxidation origin sandstone-type uranium deposits (such as the Mengqiguer and Shihongtan uranium deposits). In contrast, in the southwestern Songliao Basin, the kaolinite is enriched in ore-bearing gray sandstones [8,14–16], and the kaolinite and uranium concentrations exhibit a relatively strong positive correlation, indicating that the uranium mineralization has undergone at least one stage of acidic fluid transformation. However, the source of the acidic fluid and its genetic relationship with the tabular-shaped uranium orebody have rarely been discussed [14,15]. In fact, foreign scholars have proposed a lacustrine mudstone−humic acid genesis model and a hot brine underwater interface genesis model based on the systematical studies on the genesis of the tabular-shaped uranium orebody in the Colorado Plateau, United States [17–23]. Furthermore, it is believed that the formation of tabular-shaped uranium orebodies is related to the organic acid-rich fluid which is generated by the compaction of mudstones underlying ore-bearing layers. However, most domestic scholars consider that it is the composite genesis of both atmospheric precipitations infiltrated by interlayer oxidation and deep-sourced oil (gas) or thermal fluid, ignoring the organic acid fluid generated during the burial evolution of the overlying mudstones (coal seam or source rock) under the ore-bearing layer [14–16,24].

Therefore, the HLJ sandstone-type uranium deposit in the Songliao Basin is studied in this paper. By systematically collecting sandstone samples of different geochemical zones (oxidation zone and reduction zone) of ore-bearing strata, trace element, scanning electron microscopy (SEM), X-ray diffraction (XRD), and other analyses were carried out to identify the changes in clay minerals in different geochemical zones and the paragenetic or associated relationship with uranium minerals. Based on the regional paleoclimate and tectonic evolution, the source of kaolinite-related acidic fluids and its role in the formation of tabular-shaped uranium orebodies is discussed. The study has profound theoretical significance for the deeper understanding of the metallogenic mechanism and metallogenic model of sandstone-type uranium deposits.

## 2. Geological Setting

The Songliao Basin is the largest Mesozoic-Cenozoic petroliferous basin in Northeastern China, and it is also a fault-depression Mesozoic continental basin formed on the cratonic basement. It is further divided into seven first-order tectonic units, namely the Northern Plunge, Central Downwarp, Northeastern Uplift, Southeastern Uplift, Southwestern Uplift, Western Slope, and Kailu Downwarp [25] (Figure 1A). The HLJ uranium deposit is a tabular-shaped sandstone-type uranium deposit formed in continental fluvial facies [26]. It is located in the Qianjiadian Sag, a secondary tectonic unit across the Kailu Downwarp and Southwestern Uplift (Figure 1B). The Pre-Mesozoic basement faults, such as $F_1$, $F_8$, and $F_{12}$, occur surrounding the HLJ uranium deposit (Figure 1B). The $F_1$ fault in the south is NE trending, and controls the tectonic environment at the east of the mining area. The fault was a normal fault in the early stage, and caused the formation to uplift and erode to form the Baolongshan tectonic erosion fenster. The $F_8$ fault is located to the west of the $F_1$ fault, and is characterized by a normal fault with a NE trend (Figure 1B). This fault mainly controls the western margin of the Qianjiadian Sag and extends northward to the HLJ mining area in the north. The $F_{12}$ fault is a strike-slip normal fault, dipping to the NE with the southeast part extending through the HLJ mining area. In comparison, basement faults such as the $F_1$ fault not only penetrate the Cretaceous strata, but also connect the source rocks of the Lower Cretaceous Jiufotang Formation (Jiufotang Fm) ($K_1jf$) as a natural channel for the upward escape of deep fluid.

The sedimentary strata exposed by drilling in the HLJ mining area include the Upper Cretaceous Qingshankou ($K_2qn$), Yaojia ($K_2y$), Nenjiang ($K_2n$), Sifangtai ($K_2s$) Fms, Neogene

Taikang Fm ($N_2t$), and the Quaternary (Q) (Figure 2A). The uranium mineralization occurs in the red mottled sedimentary construction of the Lower Yaojia Fm (Figures 2B, 3 and 4). The upper and lower oxidized zones and reduced zones can be identified vertically. The ore-controlling gray sandstones are surrounded by red mottled oxidized sandstones, and the orebody mainly occurs in the medium-fine-grained gray sandstones and is a multi-stratiform and tabular-shaped orebody (Figures 3 and 4).

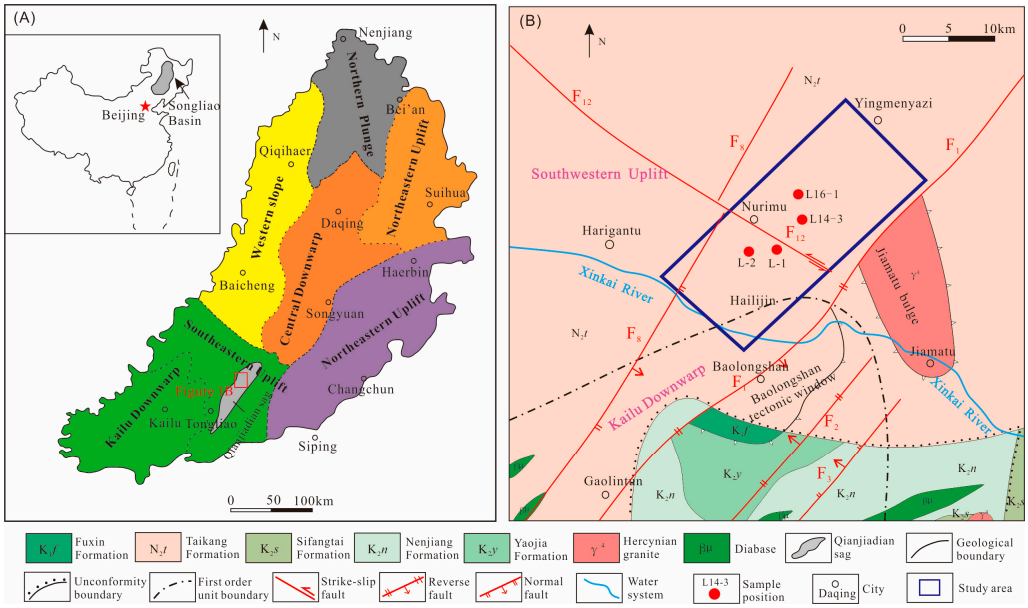


**Figure 1.** (**A**) Tectonic units of the Songliao Basin (modified from Feng et al., 2017 [25]); (**B**) pre-Quaternary geological map of the HLJ mining area.

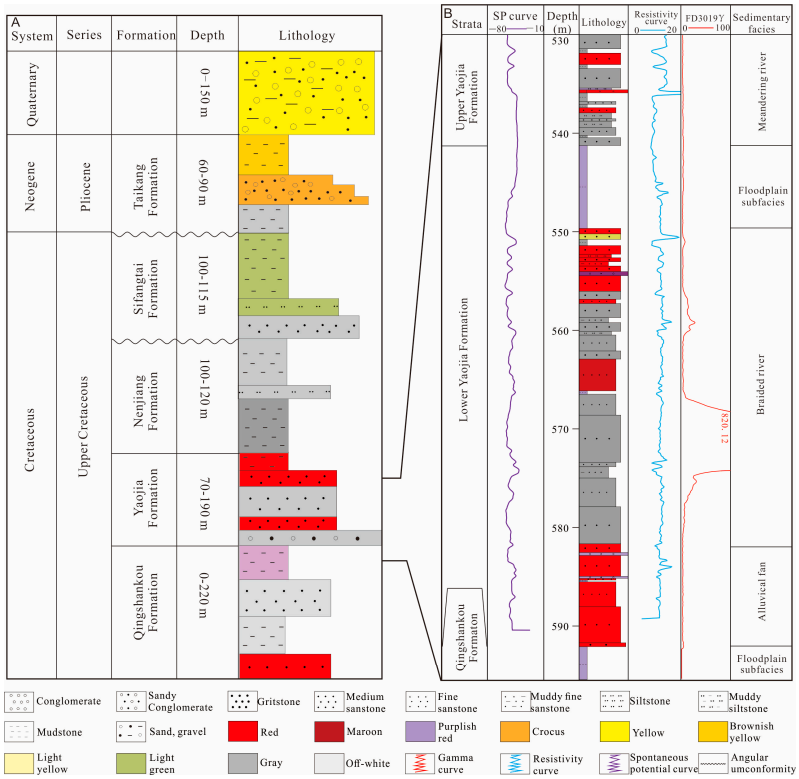


**Figure 2.** Strata histogram of the HLJ uranium deposit (**A**) and the lithology histogram of the Lower Yaojia Fm of ore-bearing strata (**B**).

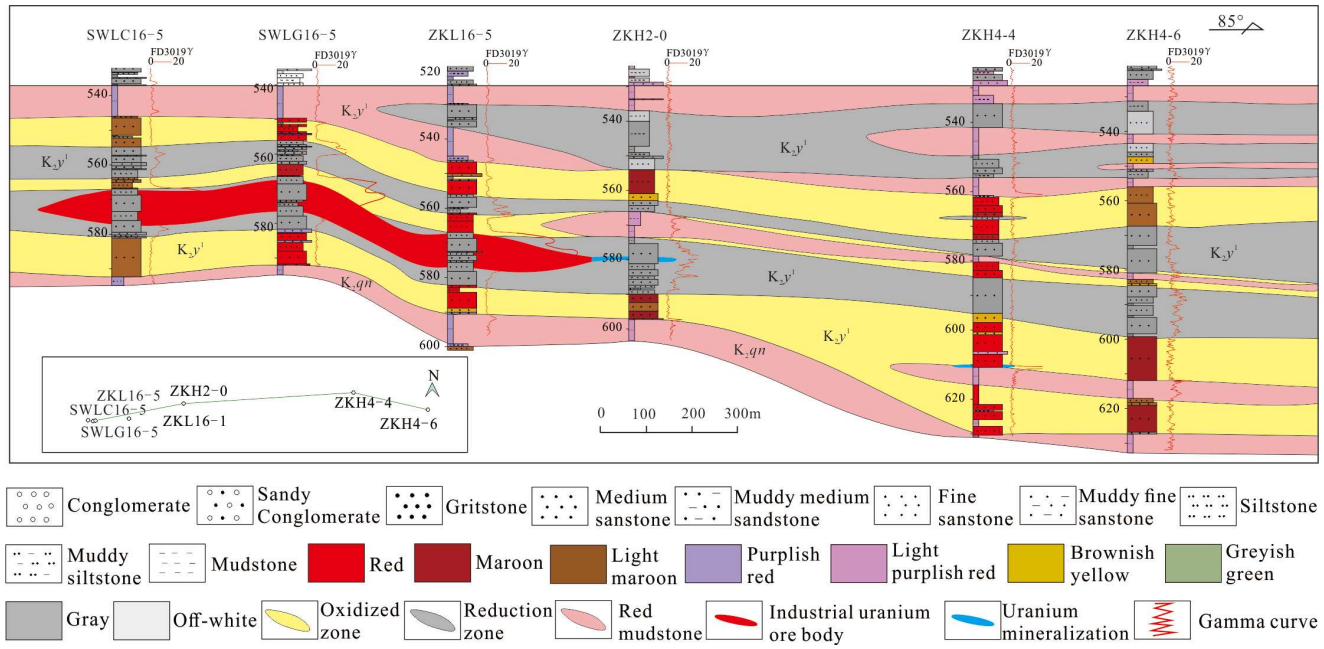


**Figure 3.** East–west trending geological cross-section of the HLJ uranium deposit.

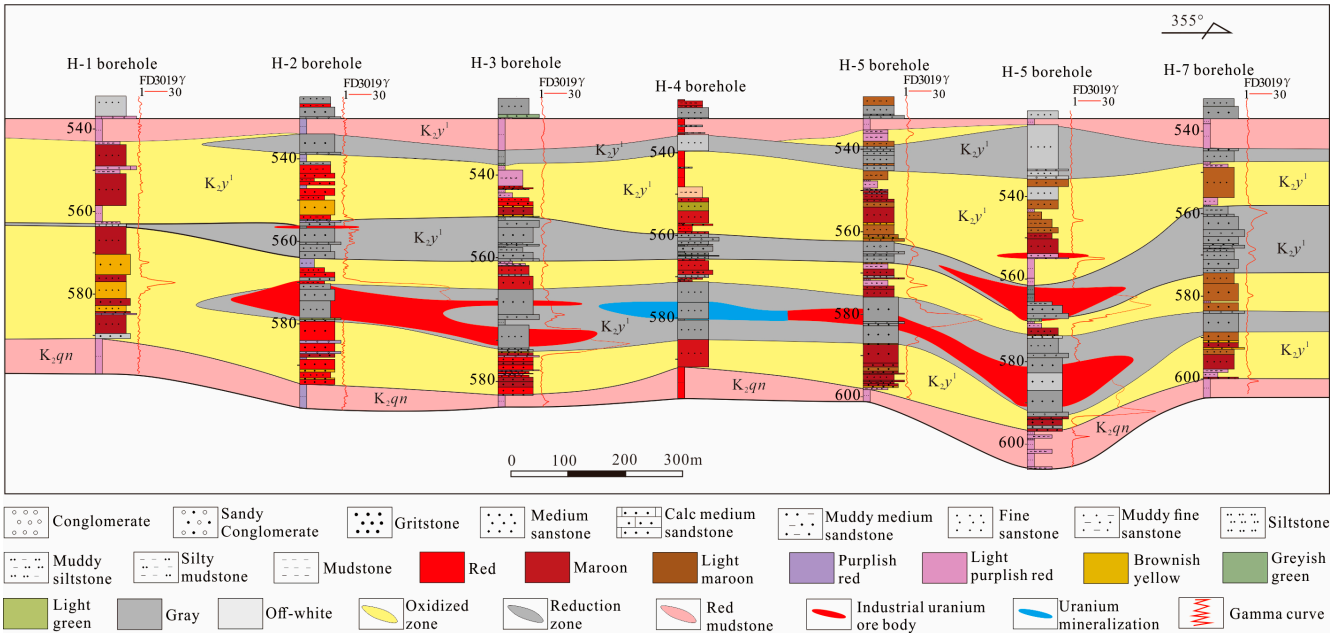


**Figure 4.** South–north trending geological cross-section of the HLJ uranium deposit.

## 3. Methods

Samples analyzed in this contribution were collected from drill hole cores of the Lower Yaojia Fm in the HLJ uranium deposit (sampling position is shown in Figure 1B), covering the oxidized sandstones, reduced zone sandstones, and ores. The petrographic analysis, trace element analysis, X-ray diffraction (XRD) analysis, scanning electron microscopy (SEM), and electron probe microanalysis (EPMA) were all conducted at the Analytical Laboratory of Beijing Research Institute of Uranium Geology (ALBRIUG). The specific analytical methods are described in the following.

### *3.1. Trace Elements Analysis*

Before testing, the oxide film, soil cement, and other impurities on the sample surface were cleaned. Samples were then rinsed and dried, and ground into 200 mesh. Trace elements were analyzed using a plasma mass spectrometer (ICP-MS). The sample processing method was as follows: Firstly, weighing 200 mg of powdered sample, mixing uniformly with 900 mg $LiBO_2$ flux, then melting in a furnace at 1000 °C. Secondly, dissolving and diluting the melt with 100 mL 4% nitric acid after the melt was cooled, and then analyzing using ICP-MS; the analysis accuracy was 5%–10%.

### *3.2. XRD Analysis*

Samples were subjected to XRD analysis at ALBRIUG using an X'Pert PROMPD X-ray diffraction system produced by Panalytical Company in Holland. The operating voltage was 40 kV and the current was 40 mA. The X-ray was suspected to be a Cu target, and the measurement angle was between 5° to 70°. During the measurement, only the edge of the samples could be taken to avoid contamination of the X-ray measuring plane. The specific analysis process refers to the implementation standard SY/T 5163-2018.

### *3.3. SEM Analysis*

The SEM analyses of 25 selected samples were carried out at ALBRIUG using a Nova Nano SEM450 scanning electron microscope, which was produced by FEI Company in Czech Republic. Samples for testing were thin sections of 1 cm × 1 cm × 1 cm cubic targets. The test plane was carbonized and numbered. The laboratory temperature was controlled at (20 ± 2) °C and the humidity was less than 80%. The main part of the instrument was always in a high-vacuum state.

### *3.4. EPMA Analysis*

The uranium minerals' composition in 3 samples with a total of 33 testing points was determined at Analytic Laboratory of Beijing Research Institute of Uranium Geology (ALBRIUG) using a JXA-8100 Electron Probe Micro Analyzer equipped with four wavelength dispersive spectrometers. The samples were first coated with a thin carbon film, and the precautions suggested by Zhang and Yang [27] were used to minimize the difference in the carbon film thickness between samples and to obtain an approximately uniform ca. 20 nm coating. The working voltage was 20 kV and the beam current was $1 \times 10^{-8}$ A. Data were corrected online using a modified ZAF (atomic number, absorption, fluorescence) correction procedure.

## 4. Results

### *4.1. Mineralogy*

Sandstones in the reduced zone are characterized by a grayish tone (Figure 5a), partly containing organic matter (Figure 5b). In contrast, the sandstones in oxidized zones show a reddish tone (Figure 5c,d). Sandstones of the reduced zone are characterized as gray or off-white, medium- to fine-grained, with relatively poor−moderate sorting and poor roundness (Figure 5e), representing a feature of near-source accumulation. The rock-forming minerals are mainly quartz (with a content of 60%–65%) and feldspar (with a content of 10%–15%), of which feldspar is composed of microcline, perthite, and a small amount of plagioclase. The debris includes intermediate-acid volcanic rocks, metaquartzite, and mica schist with a content of 20%–25%. In addition, the accessory minerals are dominated by zircon, pyrite, apatite, ankerite, dolomite, etc. Generally, uranium minerals are often observed in dissolved pores on the surface of quartz and feldspar (Figure 5f,g). Meanwhile, hematitization spots can be observed in gray sandstone (Figure 5h).

The oxidized zone sandstones mainly include red and maroon, medium- to fine-grained sandstones with a similar mineralogical composition to that of the gray sandstones. However, some differences still exist: (1) oxidized sandstones contain a large amount

of hematitization alteration (Figure 5i); and (2) oxidized sandstones lack organic matter and pyrite.

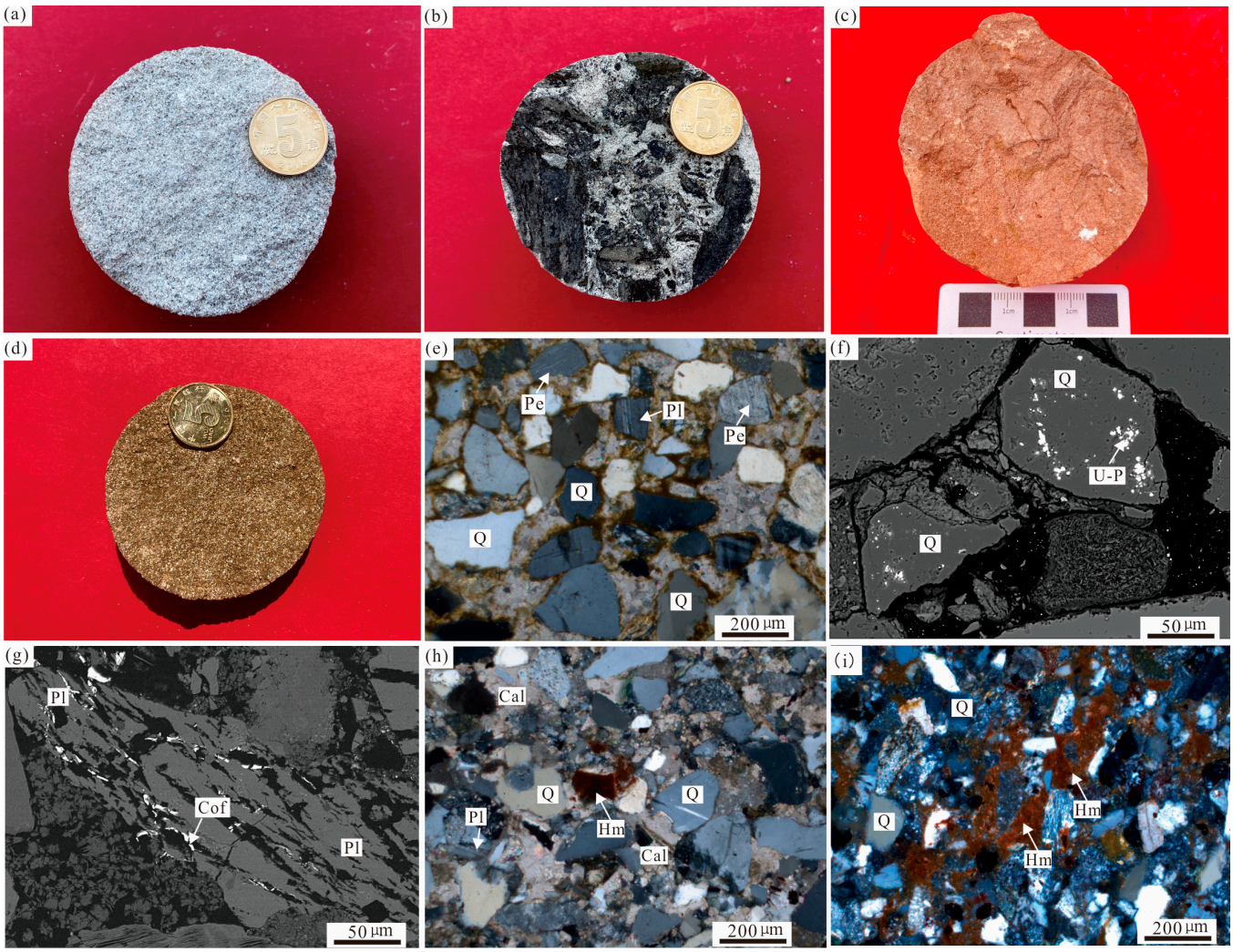


**Figure 5.** Petrographic characteristics of sandstones of the Lower Yaojia Fm in the HLJ uranium deposit. (**a**) Photograph of gray fine-grained sandstone from reduced zone; (**b**) photograph of gray fine-grained sandstone with a large amount of organic matter from reduced zone; (**c**) photograph of red fine-grained sandstone sampled from oxidized zone; (**d**) photograph of maroon coarse-grained sandstone sampled from oxidized zone; (**e**) microphotograph of gray sandstone; (**f**) uranium minerals are observed in dissolved pores on the surface of quartz (SEM image); (**g**) coffinite can be observed in dissolved pores on the surface of plagioclase (SEM image); (**h**) in reduced zone, hematitization spots can be observed in gray sandstones; (**i**) microphotograph of red sandstone, which has strong hematitization alteration and also lacks organic material and pyrites, as compared with gray sandstone. Cof—coffinite, Cal—calcite, Hm—hematitization, Pe—perthite, Pl—plagioclase, Q—quartz, U—uranium, P—phosphorus. The diameter of the coin in Figure 5a,b,d is 2 cm.

### *4.2. Clay Minerals*

The clay minerals in the Lower Yaojia Fm of the HLJ uranium deposit are composed of kaolinite, illite, and I/S (Table 1). The kaolinite is distributed on the surface of mineral particles or the micropores in a vermicular and blade-like shape (Figure 6a), while the illite is mainly in a squamiform shape. The XRD analysis results suggest that the content of kaolinite in gray sandstone is obviously higher than that in oxidized sandstone, which is the highest in the ores (Table 1, Figure 7). Scanning electron microscopy (SEM) results suggest that uranium minerals are closely related to kaolinite, and often exist in adsorbed

form on the surface of foliated and vermicular kaolinite or trapped within micropores of kaolinite, whereas coexistence between uranium minerals and illite can hardly be observed (Figure 6b–f).

Furthermore, kaolinite, illite, and I/S generally alternate with one another in gray sandstones of reduced zones (Figure 7). The content of kaolinite, illite, and I/S in oxidized zones range from 20% to 59% (ave. 49.29%), 20% to 38% (ave. 27.71%), and 14% to 42% (ave. 23%), respectively, while that in reduced zones ranges from 60% to 86% (ave. 72.1), 5% to 24% (ave. 14.1%), and 4% to 20% (ave. 13.8%).

**Table 1.** The XRD analysis results of sandstones and U content of ore-bearing strata in the HLJ uranium deposit.

| No. | Sample No. | Lithology | Depth (m) | Geological Zone | Relative Content of Clay Minerals (%) | | | U (ppm) |
|---|---|---|---|---|---|---|---|---|
| | | | | | Kl | Ilt | I/S | |
| 1 | L14-3-11 | Red fine-grained sandstone | 585.5 | Oxidized zone | 56 | 25 | 19 | 2.25 |
| 2 | L14-3-12 | Red fine-grained sandstone | 589.9 | Oxidized zone | 51 | 28 | 21 | 2.06 |
| 3 | L14-3-13 | Red fine-grained sandstone | 592.74 | Oxidized zone | 53 | 23 | 24 | 10.6 |
| 4 | L16-1-4 | Red fine-grained sandstone | 553 | Oxidized zone | 48 | 23 | 29 | 3.22 |
| 5 | L16-1-13 | Red medium-grained sandstone | 592 | Oxidized zone | 52 | 25 | 23 | 2.2 |
| 6 | L16-1-14 | Red medium-grained sandstone | 592.7 | Oxidized zone | 53 | 25 | 22 | 2.2 |
| 7 | L16-1-15 | Red medium-grained sandstone | 595 | Oxidized zone | 53 | 16 | 31 | 1.57 |
| 8 | L14-3-1 | Gray fine-grained sandstone | 562.8 | Reduced zone | 69 | 13 | 18 | 13.6 |
| 9 | L14-3-2 | Light-gray fine-grained sandstone | 567.1 | Reduced zone | 56 | 20 | 24 | 2.62 |
| 10 | L14-3-3 | Light-gray fine-grained sandstone | 569.1 | Reduced zone | 65 | 15 | 20 | 5.63 |
| 11 | L14-3-4 | Light-gray fine-grained sandstone | 570.1 | Reduced zone | 62 | 20 | 18 | 3.02 |
| 12 | L14-3-8 | Light-gray fine-grained sandstone | 580 | Reduced zone | 74 | 18 | 8 | 22.7 |
| 13 | L14-3-9 | Light-gray fine-grained sandstone | 583.5 | Reduced zone | 74 | 8 | 18 | 26.7 |
| 14 | L14-3-10 | Light-gray fine-grained sandstone | 584.5 | Reduced zone | 76 | 5 | 19 | 65.2 |
| 20 | L14-3-5 | Gray fine-grained sandstone | 575 | Ore | 74 | 14 | 12 | 137 |
| 21 | L14-3-6 | Gray fine-grained sandstone | 578.4 | Ore | 81 | 14 | 5 | 219 |
| 22 | L14-3-7 | Gray fine-grained sandstone | 578.6 | Ore | 86 | 10 | 4 | 62.8 |
| 23 | ZKL-16 | Gray medium-grained sandstone | 582.3 | Ore | 70 | 30 | / | 303 |
| 24 | ZKL-17 | Gray medium-grained sandstone | 584.3 | Ore | 82 | 11 | 7 | 1164 |
| 25 | ZKL-18 | Gray medium-grained sandstone | 583.3 | Ore | 82 | 12 | 6 | 1654 |
| 26 | ZKL1-2 | Gray fine-grained sandstone | 573 | Ore | 74 | 13 | 13 | 823 |
| 27 | ZKL1-3 | Gray fine-grained sandstone | 574 | Ore | 61 | 24 | 15 | 393 |

Notes: Kl—kaolinite, I/S—illite/smectite formation, Ilt—illite, U—uranium.

### *4.3. Trace Elements*

The average content variations in trace elements in the HLJ uranium deposit are listed in Table 2. U, Mo, Re, V, Ni, Pb, Cr, Cu, and Zn of gray sandstones in reduced zones are richer than those in oxidized zones. Furthermore, these elements are significantly more enriched in ores. In particular, the content of Mo in ore-bearing gray sandstones is almost nine times higher than that in oxidized zone sandstones. Re, Ni, Co, Zn, Cu, Pb, and V in reduced zones are significantly increased, by 323%, 60%, 72%, 30%, 44%, 34%, and 22%, respectively, compared with the sandstones in oxidized zones.

**Table 2.** Average content of trace elements of sandstone of the ore-bearing strata in the HLJ uranium deposit.

| Trace Element | Average Content of Trace Element (ppm) | | | | | | | | | | | | |
|---|---|---|---|---|---|---|---|---|---|---|---|---|---|
| Geochemical Zone | V | Cr | Co | Cu | Ni | Zn | Re | Mo | Pb | Th | U | Zr | Hf |
| Upper oxidized zone (15) | 32.41 | 16.35 | 4.45 | 7.67 | 6.97 | 44.56 | 0.01 | 0.59 | 17.73 | 9.49 | 2.76 | 134.73 | 4.96 |
| Non-ore-bearing gray sandstone (70) | 34.62 | 20.35 | 6.25 | 9.24 | 9.04 | 51.50 | 0.02 | 0.67 | 20.12 | 9.42 | 20.21 | 146.04 | 4.98 |
| Ore-bearing gray sandstone (68) | 38.67 | 19.62 | 7.65 | 11.02 | 11.15 | 58.06 | 0.23 | 6.01 | 22.48 | 9.12 | 468.70 | 137.79 | 4.21 |
| Lower oxidized zone (22) | 31.80 | 14.43 | 5.12 | 7.56 | 7.55 | 48.04 | 0.01 | 0.72 | 16.74 | 8.37 | 4.57 | 121.82 | 4.34 |

Notes: the number in bracket represents the quantity of samples.

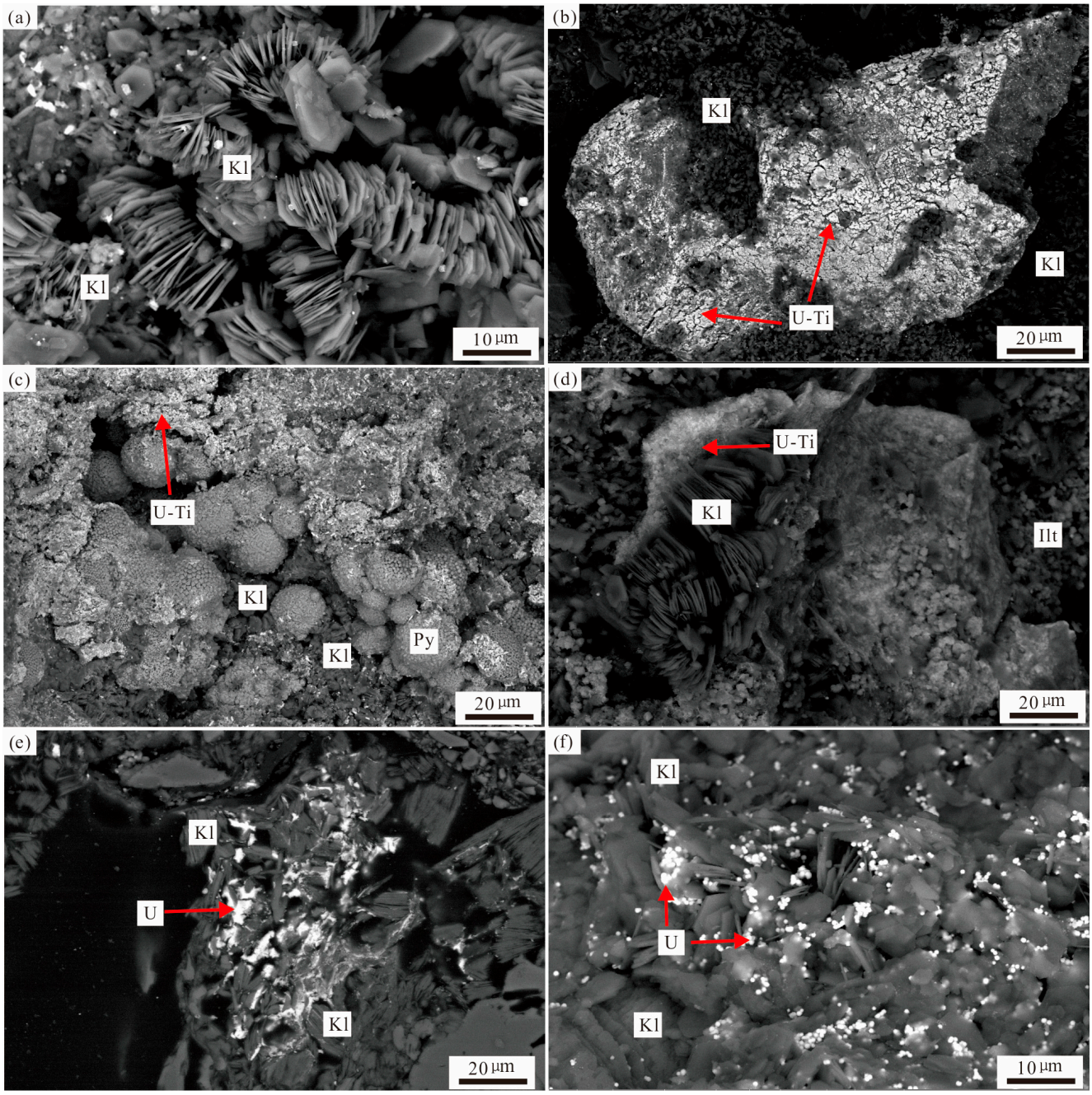


**Figure 6.** Paragenetic relationship between uranium minerals and clay minerals in HLJ uranium deposits: (**a**) kaolinite in shape of blades; (**b**) uranium and titanate minerals occur on the surface of kaolinite; (**c**) uranium, titanate, and framboid pyrite occur in the micropores of kaolinite; the formation of framboid pyrite is earlier than that of uranium; (**d**) uranium and titanate are absorbed on the surface of kaolinite, while the coexistence of uranium minerals and illite can hardly be observed; (**e**) uranium occurs in the pores of kaolinite; (**f**) the microcrystalline form of uranium is adsorbed on the surface of kaolinite. Ilt—illite, Kl—kaolinite, Py—pyrite, Ti—titanate, S—sulfur, U—uranium.

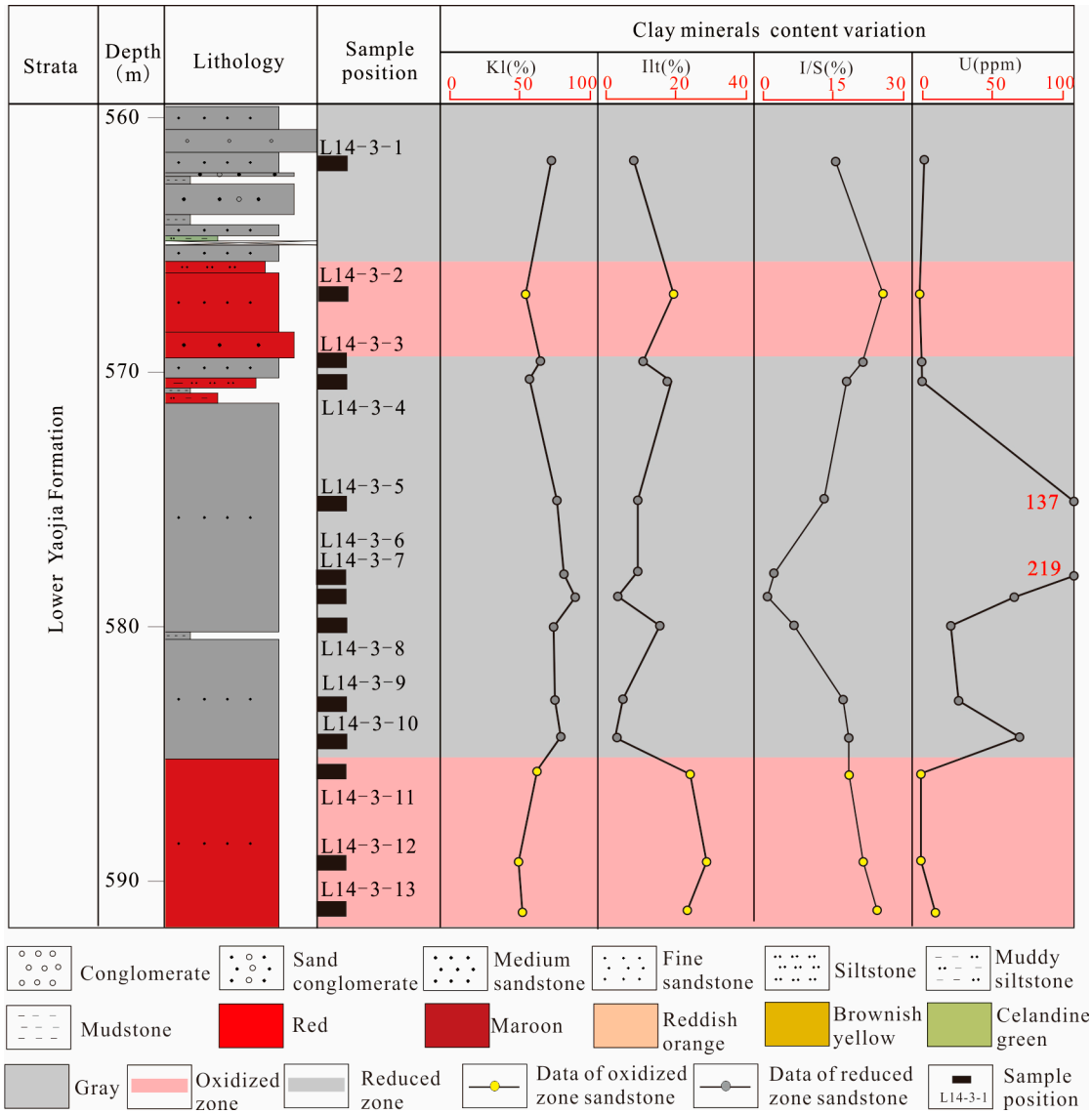


**Figure 7.** Vertical variation in clay minerals' content in sandstones of the Lower Yaojia Fm in the HLJ uranium deposit. I/S—mixed montmorillonite/illite layer, Ilt—illite, Kl—kaolinite, U-uranium.

## 5. Discussion

### *5.1. The Fluid Property and Sources Related to the Formation of Kaolinite*

The XRD analysis results of ore-bearing strata sandstones in the HLJ uranium deposit suggest that the kaolinite, illite, and I/S in ore-controlling gray sandstones alternate with one another (Table 1, Figure 7); that is, the kaolinite in gray sandstones is obviously enriched compared to that in oxidized sandstones, and reaches the highest level in the ore. This unique signature is significantly different from the enrichment of kaolinite in less oxidized sandstones of sandstone-type uranium deposits of interlayer oxidization−infiltration origin in Western China (such as the Mengqiguer uranium deposit in the Yili Basin and the Shihongtan uranium deposit in the Turpan-Hami Basin) [28–31]. Previous research indicated that the formation of kaolinite is generally related to an acidic environment with a hot and humid climate [15,32–34], whereas numerous studies have shown that the paleoclimate of the Yaojia period in the study area was dominated by an arid climate [35–41]. Obviously, the enrichment of kaolinite in ore-bearing strata of gray sandstones is not a response to paleoclimate, which has also been reported by Rong et al. (2016) [42], Li et al. (2018, 2020) [15,16], Shan et al. (2019) [34], and Li et al. (2022) [43]. Combined with the

co-existing uranium minerals and kaolinite and illite (Figure 6), it is believed that the ore-bearing sandstones of the HLJ uranium deposit have undergone at least one transformation of acidic fluids, and the transformation of I/S to kaolinite occurred during the uranium mineralization period. Previous studies suggest that the acidic fluids are derived from the upward evaporation of petroleum (gas) in the Lower Cretaceous strata underlying the ore-bearing strata [24,36,37]. The latest research shows that the enrichment of kaolinite in ore-controlling gray sandstones in the Qianjiadian uranium deposit is of epigenetic origin, which is related to acidic organic fluids formed by the upward evaporation of the Lower Cretaceous Jiufotang Fm ($K_1jf$) source rocks along the deep-seated faults connecting the overlying ore-bearing layers [14–16]. Furthermore, the temperature of the acidic organic fluids was limited to 40–120 °C by means of fluid inclusion temperature measurement [44] and H-O isotopes of kaolinite [14]. In addition, the sandstones of the Yaojia Fm in the Qianjiadian area also contain some adsorbed hydrocarbons and inclusion hydrocarbons; n-alkanes exhibit a bimodal distribution feature. The main peak carbon ranges are $C_{16}$ and $C_{22}$–$C_{25}$, and the Pr/Ph ranges from 0.51 to 0.84 [45], which reflects the source rocks formed in an anoxic environment [45–48]. In addition, the vitrinite reflectivity ($R_o$) of the adsorbed hydrocarbons and inclusion hydrocarbons ranges from 0.51% to 0.6% [45], indicating that the oil filled in the sandstones derived from a mature stage. These organic geochemistry findings manifest that the parent materials are at the submature−mature thermal evolution stage, which is consistent with the lacustrine source rocks of the Lower Cretaceous Jiufotang Formation in the Qianjiadian area [14,47,48].

As mentioned above, the $F_1$ fault, which is located in the southeast of the HLJ uranium deposit, not only penetrates the Cretaceous strata, but also connects the source rocks of the Lower Cretaceous Jiufotang Fm ($K_1jf$), which provides a natural channel for the upward escape of deep fluid. In this case, the acidic organic fluids derived from the source rocks of Jiufotang Fm escaped upward to the ore-bearing layers (Figure 8), then reduced the primary oxidized sandstones of Yaojia Fm accompanied by the reduction of $Fe^{3+}$ to $Fe^{2+}$, and finally formed large-scale secondary reduced gray sandstones. This speculation can explain the phenomenon of hematitization spots that are commonly observed in gray sandstones (Figure 5h), which are actually a residue of incomplete reduction transformation. Therefore, the authors believe that the enrichment of kaolinite in the ore-controlling gray sandstone of the HLJ uranium deposit is strongly associated with the acid organic fluids that derived from the Lower Cretaceous Jiufotang Fm source rocks escaping upward along the $F_1$ deep-seated fault.

### *5.2. Genetic Mechanism of Tabular-Shaped Uranium Orebody*

SEM analysis results suggest that the adsorption of uranium to kaolinite is significantly stronger than that to illite and I/S (Figure 6), which is in contradiction with previous studies showing the the adsorption capacity of uranium to montmorillite and illite is much greater than that of kaolinite [49,50]. Therefore, it is speculated that the acidic organic fluid related to the formation of kaolinite is also a uranium-rich fluid. Some simulation experiments in recent years have confirmed that a large amount of uranium could be excreted from the source rocks while generating and expelling hydrocarbons [15,43,51–53]. Zhang (2018) [54] even put forward the conjecture that the source rock is the uranium source. The uranium in source rocks immigrating into oilfield water can reach up to 50% under certain temperature and pressure conditions [16], as long as the continuous hydrocarbon generation of source rocks and the decomposition of saturated hydrocarbons, a reducing fluid rich in $CO_2$, $CH_4$, $H_2S$ and organic acids, can eventually be generated [43], which is a benefit to uranium and other polymetallic dissolution and migration. Consequently, the uranium migrated as either tetravalent ($UO_2$) or in the form of hydrate colloid ($UO_3 \cdot H_2O$, $UO_2 \cdot H_2O$, $U_6O_7 \cdot H_2O$), and finally precipitated and enriched in sandstones with suitable porosity and permeability [43]. Furthermore, the uranium and chloride complex ($UCl_4$) is relatively stable under reduced acidic conditions with a temperature greater than 100 °C. The solubility of $UCl_4$ decreases in an oxidized environment or as temperature decreases, and ultimately, the pitchblende

precipitates [55]. Comprehensively, sources rocks not only provide a reduced environment for uranium mineralization, but also provide uranium sources.

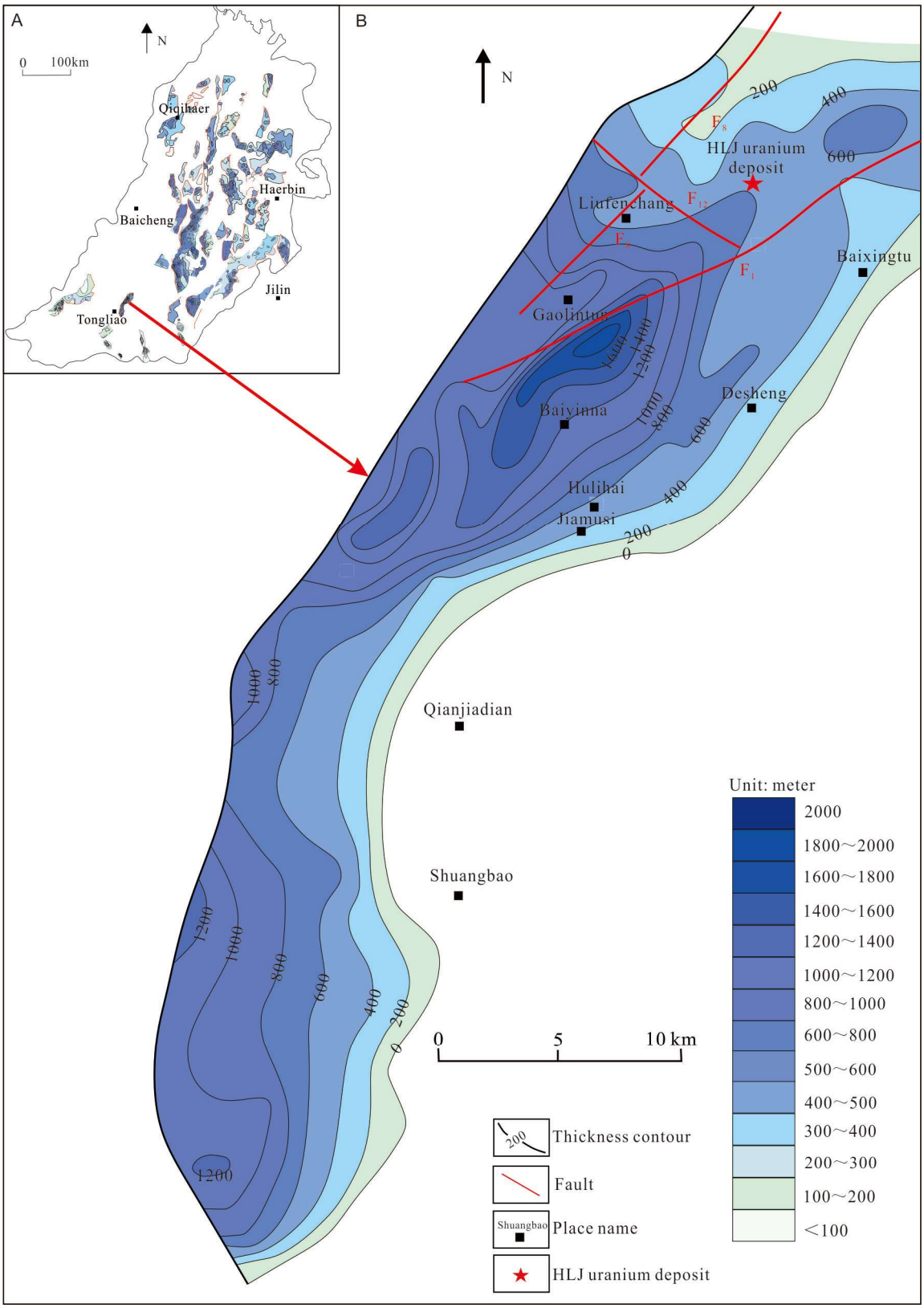


**Figure 8.** (**A**) Source rock distribution of the Lower Cretaceous, Songliao Basin, and (**B**) thickness contour map of uranium-rich source rock of Jiufotang Fm in the Qianjiadian Sag.

Actually, source rocks in the Jiufotang Fm ($K_1jf$) of the Lower Cretaceous in southwestern Songliao Basin have a large thickness and wide area; they also possess a higher uranium content of (1.52–10) $\times$ $10^{-6}$ [56–58] (Figure 8) and are enriched in Mo, Co, Zn, Pb, V, Zr, and other elements [59]. These features are consistent with the results of trace element, EMPA, and SEM analysis of ore-bearing strata sandstones in the HLJ uranium deposit. Trace elements of bulk samples indicate that the gray sandstones are generally enriched in U, Re, Mo, Co, Ni, Pb, V, Cu, and Zn, which are much more enriched in ores (Table 2). Generally, it is relatively difficult to precipitate and enrich these elements under atmospheric conditions. Conversely, they are more likely to be derived from deep-sourced acidic fluids [43]. The SEM analysis demonstrated that the uranium commonly coexists with Zr, Ti, Pb, and P (Figures 9 and 10). The EMPA analysis supported a similar conclusion, i.e., the pitchblende contains 62.72%–71.11% of $UO_2$, followed by $TiO_2$, $ZrO_2$, CaO, $P_2O_5$, PbO, $As_2O_5$, $SiO_2$, $Ce_2O_3$, etc. (Table 3).

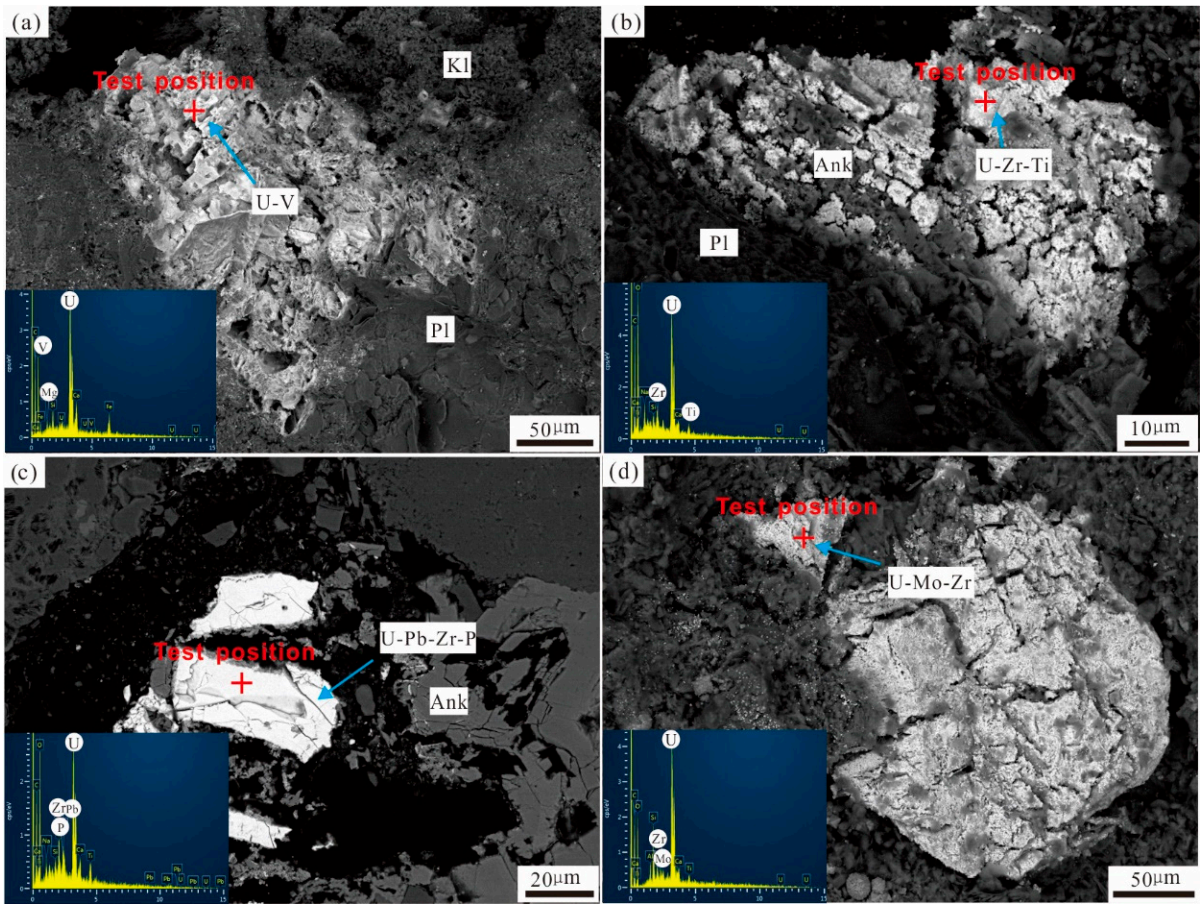


**Figure 9.** The co-existence relationship between uranium minerals and polymetallic elements in the HLJ uranium deposit: (**a**) uranium and vanadium co-exist in the intergranular pores; (**b**) uranium, zircon, and titanate co-exist in the micropores of ankerite; (**c**) uranium, zircon, lead, and phosphorus co-exist around the ankerite; (**d**) uranium, zircon, and molybdenum co-exist in the micropores of kaolinite. Ank—Ankerite, Kl—kaolinite, Mo—molybdenum, P—phosphorus, Pb—lead, Pl—plagioclase, Ti—titanate, U—uranium, V—vanadium, Zr—zircon.

It is concluded that the genesis of the tabular-shaped orebody of the HLJ sandstone-type uranium deposit is strongly related to the upward exudation of uranium-rich acidic reduced organic fluids from deep source rocks along the deep-seated fault connecting the overlying target layers. At the end of the Nenjiang movement, the deep-seated $F_1$ fault was subjected to tectonic inversion under the regional subduction and compression, which not only caused the denudation and erosion of sediments in the Qianjiadian area,

but formed the Baolongshan tectonic erosion fenster. Meanwhile, the upward exudation of uranium-rich and polymetallic-rich reduced fluids along the $F_1$ fault to the primary oxidized sediments in the Lower Yaojia Fm, and the oxidized sandstones were reduced to gray sandstones with a bead-like and lenticular shape (Figure 3). As the temperature and pressure decreased, the Eh and pH values of the reduced fluids changed, resulting in the decomposition of uranium-rich organic fluids under the chemical action of oxidation, decarbonation, dehydration, and desulfurization, and leading to the decrease in the solubility of the ore-forming elements. Consequently, the enrichment and precipitation of uranium and polymetallic in sandstones with suitable porosity and permeability occurs, and eventually, the uranium was mineralized (Figure 11). Necessarily, the occurrence of deep uranium-rich organic fluid exudation and mineralization does not rule out the superimposed transformation of uranium mineralization by phreatic oxidation or local interlayer redox.

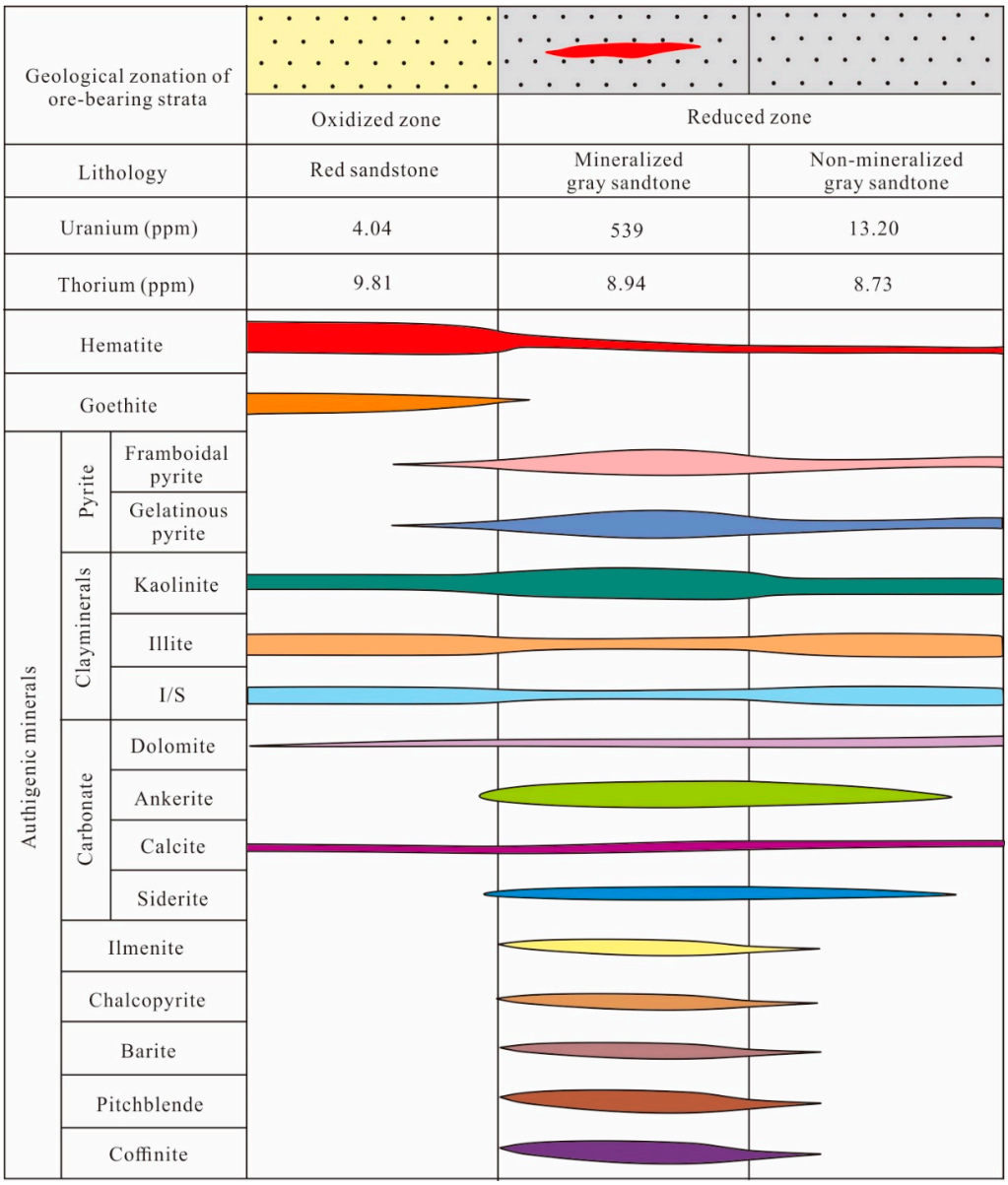


**Figure 10.** Concentrations of U and Th, and uranium-related minerals of the ore-bearing strata in the HLJ uranium deposit (modified from Rong et al., 2019 [60]).

**Table 3.** Electron probe microanalysis results of pitchblende in the HLJ uranium deposit (%).

| Test No. | $Y_2O_3$ | $SiO_2$ | $TiO_2$ | $K_2O$ | $Na_2O$ | MgO | FeO | CaO | $As_2O_5$ | $Al_2O_3$ | $Ce_2O_3$ |
|---|---|---|---|---|---|---|---|---|---|---|---|
| 1 | 0.47 | 0.82 | 4.68 | 0.13 | 0.68 | 0.35 | 0.39 | 3.68 | 0.89 | 0.14 | 0.41 |
| 2 | 0.56 | 0.71 | 4.32 | 0.13 | 1.93 | 0.29 | 0.62 | 3.89 | 1.14 | / | 0.38 |
| 3 | 0.51 | 0.74 | 4.56 | 0.12 | 2.20 | 0.25 | 0.36 | 3.02 | 1.06 | / | 0.32 |
| 4 | 0.51 | 0.70 | 4.37 | 0.13 | 1.62 | 0.35 | 0.31 | 3.02 | 0.83 | 0.03 | 0.37 |
| 5 | 0.61 | 0.76 | 4.55 | 0.34 | 2.94 | 0.28 | 0.43 | 4.42 | 1.14 | 0.05 | 0.52 |
| **Test No.** | **$P_2O_5$** | **$Pr_2O_3$** | **$ZrO_2$** | **$Nd_2O_3$** | **$ThO_2$** | **$Cr_2O_3$** | **$UO_2$** | **CuO** | **PbO** | **$La_2O_3$** | **Total** |
| 1 | 2.99 | 0.03 | 4.30 | 0.31 | 0.17 | / | 69.11 | 0.16 | 1.38 | 0.11 | 91.20 |
| 2 | 2.87 | 0.04 | 4.06 | 0.36 | 0.23 | / | 67.35 | 0.07 | 0.49 | / | 89.44 |
| 3 | 2.45 | 0.04 | 3.60 | 0.33 | 0.26 | / | 62.72 | 0.07 | 2.81 | 0.11 | 85.53 |
| 4 | 2.80 | / | 3.55 | 0.51 | 0.21 | 0.04 | 67.11 | / | 1.86 | / | 88.32 |
| 5 | 2.90 | / | 4.14 | 0.42 | 0.31 | / | 71.11 | 0.06 | 0.16 | / | 95.14 |

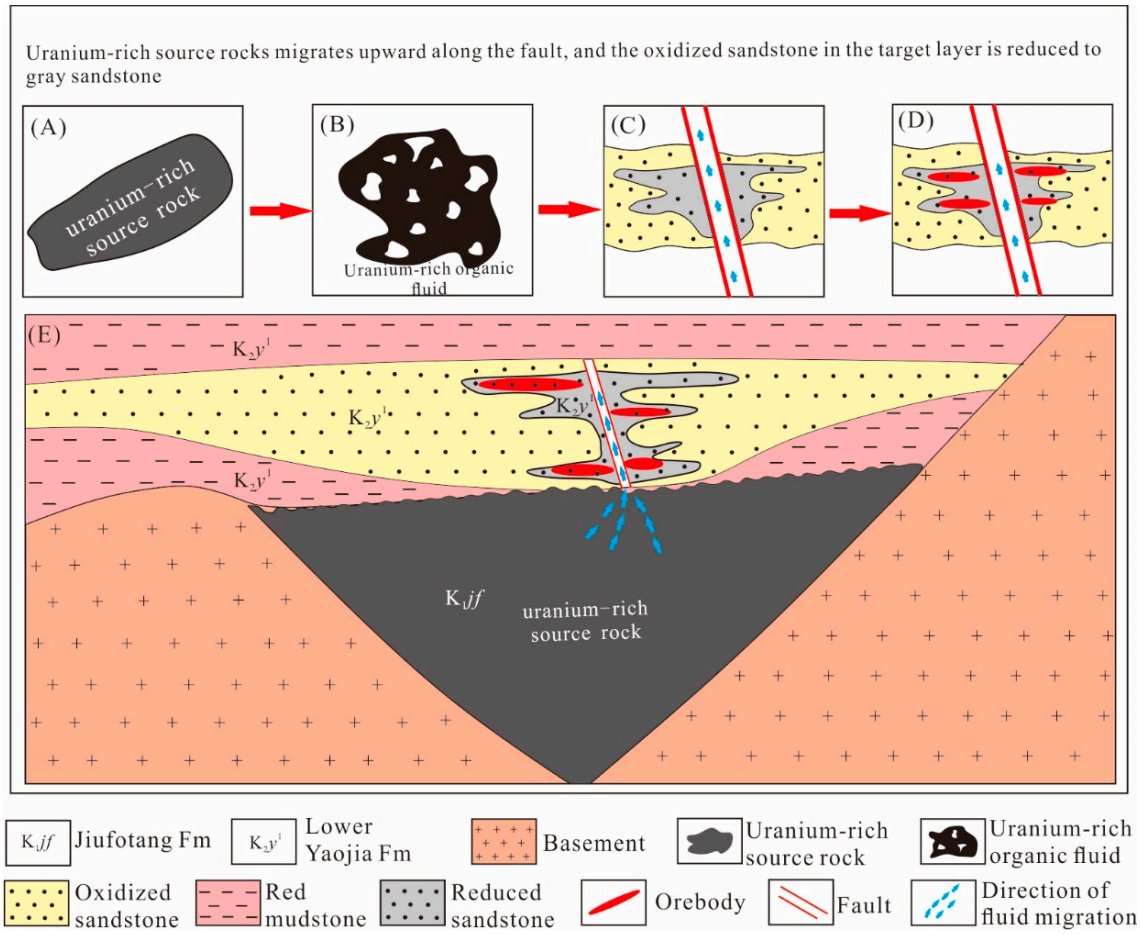


**Figure 11.** Migration pattern of uranium-rich organic fluids and exudative uranium metallogenic model of the HLJ uranium deposit. (**A**) The uranium-rich source rocks of the Lower Cretaceous Jiufotang Formation. (**B**) The source rocks generate a large quantity of uranium-rich organic fluids while generating and expelling hydrocarbons. (**C**) The upward exudation of uranium-rich reduced fluids along the fault to the primary oxidized sediments, and the oxidized sandstones were reduced to gray sandstones with a bead-like and lenticular shape. (**D**) With the decrease in temperature and pressure, the enrichment and precipitation of uranium in gray sandstones with suitable porosity and permeability occurs, and eventually, the uranium mineralizes. (**E**) Exudative uranium metallogenic model of the HLJ uranium deposit.

## 6. Conclusions

(1) The kaolinite content in gray sandstone is obviously higher than that in oxidized sandstone, and is highest in the ore. Kaolinite, illite, and I/S alternate with one another in gray sandstones of reduced zones.
(2) The ore-bearing sandstones of the HLJ uranium deposit have undergone at least one transformation of acidic fluids, and the transformation of I/S to kaolinite occurred during the uranium mineralization period.
(3) The genesis of the tabular-shaped orebody of the HLJ sandstone-type uranium deposit is strongly related to the upward exudation of uranium-rich acidic reduced organic fluids from deep source rocks along the deep-seated fault connecting the overlying target layers.

**Author Contributions:** Conceptualization, M.T. and Z.L.; Investigation, M.T., L.J., J.N., J.L., H.H. and G.T.; Writing—original draft, M.T.; Writing—review and editing, Y.Z. and L.J. All authors have read and agreed to the published version of the manuscript.

**Funding:** This research is jointly sponsored by Integrated Research and Development Project "Multi-coupling Geological Metallogenesis and Spatial-Temporal Positioning of Sandstone-type Uranium Deposit", China National Nuclear Corporation Ltd. (No. 2021-143).

**Data Availability Statement:** Data is contained within the article.

**Acknowledgments:** We sincerely thank Haitao Wang, Shaohua Zhang of No. 243 Geological Party of CNNC for their selfless help in fieldwork and sampling. We also appreciate Xiaotong Liu and Apeng Yu at Analytical Laboratory of Beijing Research Institute of Uranium Geology for providing accurate and reliable analysis data. We would also like to thank Longsheng Yi at the Beijing Research Institute of Uranium Geology for polishing the language in the paper. The anonymous reviewers are also thanked for their constructive comments and suggestions on this manuscript.

**Conflicts of Interest:** The authors declare no conflict of interest.

## References

1. Zhao, L.; Cai, C.F.; Jin, R.S.; Li, J.G.; Li, H.L.; Wei, J.L.; Guo, H.; Zhang, B. Mineralogical and Geochemical Evidence for Biogenic and Petroleum-related Uranium Mineralization in the Qianjiadian Deposit, NE China. *Ore Geol. Rev.* **2018**, *101*, 273–292. [CrossRef]
2. Cheng, Y.H.; Wang, S.Y.; Zhang, T.F.; Teng, X.M.; Ao, C.; Jin, R.S.; Li, H.L. Regional Sandstone-type Uranium Mineralization Rooted in Oligo-Miocene Tectonic Inversion in the Songliao Basin, NE China. *Gondwana Res.* **2020**, *88*, 88–105. [CrossRef]
3. Li, Z.Y.; Zhang, J.D.; Qin, M.K.; Fan, H.H. *Uranium Metallogenic Model in China*; Geological Publishing House: Beijing, China, 2014; pp. 3–15. (In Chinese)
4. Li, Z.Y.; Qin, M.K.; Fan, H.H.; Cai, Y.Q.; Guo, D.F.; Ye, F.W.; Fan, G.; Liu, X.Y. The Main Process of Uranium Mining Geology Science and Technology in the Past 10 Years. *Bull. Mineral. Petrol. Geochem.* **2021**, *40*, 845–857, (In Chinese with English abstract).
5. Yang, D.G.; Wu, J.H.; Nie, F.J.; Bonnetti, C.; Xia, F.; Yan, Z.B.; Cai, J.F.; Wang, C.D.; Wang, H.T. Petrogenetic Constraints of Early Cenozoic Mafic Rocks in the Southwest Songliao Basin, NE China: Implications for the Genesis of Sandstone-hosted Qianjiadian Uranium Deposits. *Minerals* **2020**, *10*, 1014–1029. [CrossRef]
6. Luo, Y.; He, Z.B.; Ma, H.F.; Sun, X. Metallogenic Characteristics of Qianjiadian Sandstone Uranium Deposit in Songliao Basin. *Miner. Depos.* **2012**, *31*, 391–400, (In Chinese with English abstract).
7. Pang, Y.Q.; Chen, X.L.; Fang, X.H.; Sun, Y. Discussion on the Interlayer Oxidation and Uranium Metallogenesis in Qianjiadian Uranium Deposit, Songliao Basin. *Uranium Geol.* **2010**, *26*, 9–16, (In Chinese with English abstract).
8. Ding, B.; Liu, H.X.; Liu, Z.Y.; Jia, L.C.; Zhang, Z.M.; Huang, S.H. Study of the Ore-controlling Function and Metallogenic Model of Local Excretion Sources in Sandstone-type Uranium Deposits in the Southwestern Songliao Basin. *Acta Geol. Sin.* **2021**, *95*, 3820–3827, (In Chinese with English abstract).
9. Li, Z.Y.; Fang, X.H.; Cheng, A.P.; Ou, G.X.; Xiao, X.J.; Sun, Y.; Liu, C.Y.; Wang, Y. Origin of Gray-green Sandstone in Ore Bed of Sandstone Type Uranium Deposit in North Ordos Basin. *Sci. China Ser. D Earth Sci.* **2007**, *50*, 165–173. [CrossRef]
10. Zhang, X. Study on the Genesis of Mengqiguer Uranium Deposit in the Southern Margin of Yili Basin. Master's Thesis, Beijing Research Institute of Uranium Geology, Beijing, China, 2012; pp. 40–60, (In Chinese with English abstract).
11. Hou, B.H.; Keeling, J.; Li, Z.Y. Paleovalley-related Uranium Deposit in Australia and China: A Review of Geological and Exploration Models and Methods. *Ore Geol. Rev.* **2017**, *88*, 201–234. [CrossRef]
12. Zhang, F.; Jiao, Y.Q.; Wang, S.M.; Wu, L.Q.; Rong, H. Origin of Dispersed Organic Matter within Sandstones and Its Implication for Uranium Mineralization: A Case Study from Dongsheng Uranium Ore Field in China. *J. Earth Sci.* **2022**, *33*, 325–341. [CrossRef]

13. Cuney, M.; Mercadier, J.; Bonnetti, C. Classification of Sandstone-related Uranium Deposits. *J. Earth Sci.* **2022**, *33*, 236–256. [CrossRef]
14. Si, Q.H.; Li, J.G.; Zhang, B.; Miao, P.S.; Li, H.L.; Cao, M.Q.; Zhu, Q. Characteristics and H-O Isotopes of Kaolinite in the Uranium-bearing Rocks from the Yaojia Formation, Qianjiadian Depression and Its Implication. *Geotecton. Metallog.* **2020**, *44*, 667–681, (In Chinese with English abstract).
15. Li, J.G.; Jin, R.S.; Zhang, B.; Miao, P.S.; Yang, K.; Li, H.L.; Wei, J.L.; Ao, C.; Cao, M.Q.; Zhang, H.L.; et al. Characteristics of Primary Clay Minerals in the Upper Cretaceous Yaojia Formation of Southwest Songliao Basin and Their Significance. *Acta Geosci. Sin.* **2018**, *39*, 295–305, (In Chinese with English abstract).
16. Li, J.G.; Zhang, B.; Jin, R.S.; Si, Q.H.; Miao, P.S.; Li, H.L.; Cao, M.Q.; Wei, J.L.; Chen, Y. Uranium Mineralization of Coupled Supergene Oxygen-uranium Bearing Fluids and Deep Acidic Hydrocarbon Bearing Fluids in the Qianjiadian Uranium Deposits, Kailu Basin. *Geotecton. Metallog.* **2020**, *44*, 576–589, (In Chinese with English abstract).
17. Adams, S.S. *Organic-related Alteration and Authigenesis Associated with Epigenetic-humate Sandstone Uranium Deposits, San Juan Basin, New Mexico*; Denver Regional Exploration Geologists Society: Lakewood, CO, USA, 1986; pp. 205–212.
18. Turner-Peterson, C.E.; Fishman, N.S. Geologic Synthesis and Genetic Models for Uranium Mineralization in the Morrison Formation, Grants Uranium Region, New Mexico. *Am. Assoc. Pet. Geol. Bull.* **1986**, *69*, 1999–2020.
19. Sanford, R.F. Hydrogeology of An Ancient Arid Closed Basin: Implications for Tabular Sandstone-hosted Uranium Deposit. *Geology* **1990**, *18*, 1099–1102. [CrossRef]
20. Sanford, R.F. A New Model for Tabular-type Uranium Deposits. *Econ. Geol.* **1992**, *87*, 2041–2055. [CrossRef]
21. Sanford, R.F. A Quantitative Model of Ground-water Flow during Formation of Tabular Sandstone Uranium Deposits. *Econ. Geol.* **1994**, *89*, 341–360. [CrossRef]
22. Northrop, H.R.; Goldhaber, M.B. Genesis of the Tabular-type Vanadium-uranium Deposits of the Henry Basin, Utah. *Econ. Geol.* **1990**, *85*, 215–269. [CrossRef]
23. Hall, S.M.; Van Gosen, B.S.; Zielinski, R.A. Sandstone-hosted Uranium deposits of the Colorado Plateau, USA. *Ore Geol. Rev.* **2023**, *155*, 39. [CrossRef]
24. Cai, J.F.; Yan, Z.B.; Zhang, L.L. Relationship Between Grey Sandstone and Uranium Mineralization in Yaojia Formation of Upper Cretaceous in Tongliao, Inner Mongolia. *J. East China Univ. Technol.* **2018**, *41*, 328–335, (In Chinese with English abstract).
25. Feng, Q.Z.; Yildirim, D.; Han, L.C.; Shu, F.Y.; Qi, A.M. Structural Architecture and Stratigraphic Record of Late Mesozoic Sedimentary Basins in NE China: Tectonic Archives of the Late Cretaceous Continental Margin Evolution in East Asia. *Earth-Sci. Rev.* **2017**, *171*, 598–620. [CrossRef]
26. International Atomic Energy Agency. *Descriptive Uranium Deposit and Mineral System Models*; International Atomic Energy Agency: Vienna, Austria, 2020; pp. 165–180.
27. Zhang, R.X.; Yang, S.Y. A Mathematical Model for Determining Carbon Coating Thickness and Its Application in Electron Probe Microanalysis. *Microsc. Microanal* **2016**, *22*, 1374–1380. [CrossRef] [PubMed]
28. Liu, H.X.; Ding, B.; Liu, Z.Y.; Zhang, X.; Pan, C.Y. Genesis of Strong Kaolinization in Ore-bearing Sandstone from Mnegqiguer uranium deposit, Yili Basin, China. *Acta Mineral. Sin.* **2017**, *37*, 40–48, (In Chinese with English abstract).
29. Ding, B.; Liu, H.X.; Li, P.; Wang, M.M.; Jiang, H.; Zhang, X.; Pan, C.Y. The Organic-inorganic Fluid Coupling Uranium Mineralization in the Southern Margin of Yili Basin. *Chin. J. Geol.* **2017**, *52*, 871–894, (In Chinese with English abstract).
30. Ding, B.; Liu, H.X.; Li, P.; Zhang, H.J.; Zhang, B.; Pan, C.Y. The Feature of Diagenetic Alteration of Ore-bearing Sandstone in Mengqiguer Uranium Deposit, Yili Basin, and the Effect of Diagenetic and Mineralization of Its Organic-inorganic Fluid. *Geol. Rev.* **2018**, *6*, 150–165, (In Chinese with English abstract).
31. Ding, B.; Liu, H.X.; Li, P.; Jiang, H.; Zhang, H.J.; Zhang, B. The Genetic Mechanism of Kaolinite in Ore-bearing Sandstone in the Mengqiguer Uranium deposit, Yili, and Its Relation with Uranium mineralization. *Acta Geol. Sin.* **2019**, *93*, 2021–2036, (In Chinese with English abstract).
32. Sun, Q.F.; Collin, C.; Zhang, J.W. A Discussion on the Factors Affecting Formation and Quantity of Clay Minerals in Climatic and Environmental Researches. *Acta Petrol. Mineral.* **2011**, *30*, 291–300, (In Chinese with English abstract).
33. Zhang, Z.Y.; Huang, L.; Lu, S.; Fu, Q.L. Characteristics of Clay Minerals in the Zonal Soil from Two Kinds of Parent Rock. *J. Huazhong Agric. Univ.* **2015**, *34*, 51–58, (In Chinese with English abstract).
34. Shan, Z.B.; Lei, A.G.; Song, B.R.; Ao, C.; Yang, S.L.; Han, H.D. Features of Clay Minerals in the Upper Cretaceous Yaojia Formation Sandstones of the Qianjiadian Area in the Songliao Basin and Its Relation to Uranium Mineralization. *Geol. China* **2019**, *49*, 271–283, (In Chinese with English abstract).
35. Luo, Y.; Ma, H.F.; Xia, Y.L.; Zhang, Z.G. Geologic Characteristics and Metallogenic Model of Qianjiadian Uranium Deposit in Songliao Basin. *Uranium Geol.* **2007**, *23*, 193–200, (In Chinese with English abstract).
36. Pang, Y.Q.; Xiang, W.D.; Li, T.G.; Chen, X.L.; Xia, Y.L. Discussion on the Origin of Bleached sandstone of Qianjiadian Uranium Deposit. *World Nucl. Geosci.* **2007**, *24*, 142–146+171, (In Chinese with English abstract).
37. Lin, J.R.; Tian, H.; Dong, W.M.; Xia, Y.L.; Zheng, J.W.; Ou, G.X.; Pang, Y.Q. Characteristics of Sulfur Isotope During the Epigenetic Alteration of Oil-gas and Coalbed Methane in the Southeastern Songliao Basin. *World Nucl. Geosci.* **2009**, *26*, 63–67, (In Chinese with English abstract).

38. Chamberlain, C.P.; Wan, X.Q.; Graham, S.A.; Carroll, A.R.; Doebbert, A.C.; Sageman, B.B.; Blisniuk, P.; Kent-Corson, M.L.; Wang, Z.; Wang, C.S. Stable Isotopic Evidence for Climate and Basin Evolution of the Late Cretaceous Songliao basin, China. *Palaeogeogr. Palaeoclimatol. Palaeoecol.* **2021**, *385*, 106–124. [CrossRef]
39. Wan, X.Q.; Zhao, J.; Scott, R.W.; Wang, P.J.; Feng, Z.H.; Huang, Q.H.; Xi, D.P. Late Cretaceous Stratigraphy, Songliao Basin, NE China: SK1 cores. *Palaeogeogr. Palaeoclimatol. Palaeoecol.* **2013**, *385*, 31–43. [CrossRef]
40. Cao, H.R.; Lei, Y.; Wang, X.Y.; Guo, X.L. Late Cretaceous Paleoclimate and Paleoenvironment in the Songliao Basin, China. *J. Paleolimnol.* **2021**, *66*, 313–331. [CrossRef]
41. Xiao, J.; Qin, M.K.; Guo, Q.; Yan, Z.L.; Jia, L.C.; Liu, X.; Xing, Z.C. Red-colored Uranium Target Horizon Reclassification and Its Significance in Qianjiadian Uranium Deposit and Surrounding Area. *Earth Sci.* **2021**, 1–25, (In Chinese with English abstract).
42. Rong, H.; Jiao, Y.Q.; Wu, L.Q.; Ji, D.M.; Li, H.L.; Zhu, Q.; Cao, M.Q.; Wang, X.M.; Li, Q.C.; Xie, H.L. Epigenetic Alteration and Its Constrains on Uranium Mineralization from the Qianjiadian Uranium deposit, Southern Songliao Basin. *Earth Sci.* **2016**, *41*, 153–166, (In Chinese with English abstract).
43. Li, Z.Y.; Liu, W.S.; Li, W.T.; Li, X.D.; Qin, M.K.; Cai, Y.Q.; Zhang, Y.L.; He, S.; Wu, Q.B.; Qiu, L.F.; et al. Exudative Metallogeny of the Hadatu Uranium Deposit in the Erlian Basin, Inner Mongolia. *Geol. China* **2022**, *49*, 1009–1047, (In Chinese with English abstract).
44. Nie, F.J.; Yan, Z.B.; Xia, F.; Li, M.G.; Lu, Y.Y.; Cai, J.F.; Guo, F.N.; Ning, J. Hot Fluid Flows in the Sandstone- type Uranium Deposit in the Kailu Basin, Northeast China. *Geol. Bull. China* **2017**, *36*, 1850–1866, (In Chinese with English abstract). [CrossRef]
45. Zhao, L.; Chen, H.; Cai, C.F.; Jin, R.S.; Wei, J.L. Geochemical Characteristics of Hydrocarbons in Ore-rich Sandstones in the Qianjiadian Uranium Deposit, Southwestern Songliao Basin. *Geol. Bull. China* **2022**, *41*, 498–508, (In Chinese with English abstract).
46. Didy, B.M.; Simoneit, B.R.T.; Brassell, S.C.; Eglinton, G. Organic Geochemical Indicators of Palaeoenvironmental Conditions of Sedimentation. *Nature* **1978**, *272*, 216–222. [CrossRef]
47. Li, H.T.; Wu, S.X.; Cai, C.F.; Luo, X.R. Forming Process of Petroleum-related Sandstone-type Uranium Ore: Example from Qianjiadian Uranium Deposit. *Geochemica* **2008**, *37*, 523–532, (In Chinese with English abstract).
48. Li, H.T.; Wu, S.X.; Cai, C.F.; Luo, X.R.; Bao, R.M. Geochemical Characteristics and Origin of Inclusions and Adsorbed Hydrocarbons in Yaojia Formation Sandstones in Qianjiadian Area, the Kailu Basin. *Pet. Geol. Exp.* **2008**, *30*, 375–381, (In Chinese with English abstract).
49. Xiu, X.Q.; Zhang, Y.Y. Experimental Study on Adsorption of Uranium by Clay Minerals. *Acta Mineral.* **2013**, *33*, 574, (In Chinese with English abstract).
50. Liao, R.; Wang, X.Y.; Yang, L.H.; Cheng, K. Research Progress on Factors Affecting the Adsorption of Uranium by Clay Minerals. *Guangzhou Chem. Ind.* **2017**, *45*, 10–12+27. (In Chinese)
51. Ma, Y.P.; Liu, C.Y.; Wang, J.Q.; Zhao, J.F.; Fang, J.J.; Gui, X.J.; Yu, L. Effects of Hydrocarbon Migration and Dissipation in Later Reformation of a Basin: Formation of Mesozoic Bleached Sandstone in Northeastern Ordos Basin. *Oil Gas Geol.* **2006**, *27*, 233–238+243, (In Chinese with English abstract).
52. Ma, Y.P.; Liu, C.Y.; Si, W.L.; Wu, J. Indication of Petrologic Records of Fluid-rock Interaction to Migration and Escaping of Hydrocarbons in Northeastern Ordos Basin. *J. Xi'an Shiyou Univ.* **2014**, *29*, 37–42+49, (In Chinese with English abstract).
53. Wu, B.L.; Wei, A.J.; Liu, C.Y.; Song, Z.S.; Hu, L.; Wang, D.; Cun, X.N.; Sun, L.; Luo, J.J. Stable Isotope Tracing on the Formation of White Sandstone in Yan'an Group, Northern Ordos Basin, and Its Geological Significance. *Earth Sci. Front.* **2015**, *22*, 205–214, (In Chinese with English abstract).
54. Zhang, W.L. Hydrocarbon Source Rock = Uranium Source Rock: New Thinking About Metallogenic Material Source of Sandstone Type Uranium Deposit. *Miner. Resour. Geol.* **2018**, *32*, 1–7, (In Chinese with English abstract).
55. Timofeev, A.; Migdisov, A.A.; Williams-Jones, A.E.; Roback, R.; Nelson, A.T.; Xu, H.W. Uranium Transport in Acidic brines Under Reducing Conditions. *Nat. Commun.* **2018**, *9*, 1–7. [CrossRef]
56. Feng, Z.H.; Fang, W.; Li, Z.G.; Wang, X.; Huo, Q.L.; Huang, C.Y.; Zhang, J.H.; Zeng, H.S. Depositional Environment of Terrestrial Petroleum Source Rocks and Geochemical Indicators in the Songliao Basin. *Sci China Earth Sci* **2011**, *41*, 1253–1267, (In Chinese with English abstract).
57. Wu, Y.M.; Yin, Z.J. Evaluation of Source Rocks in Manghan Depression of Kailu Basin and Its Exploration Potential. *J. Southwest Pet. Univ.* **2011**, *33*, 37–41, (In Chinese with English abstract).
58. Wang, Z.H.; Li, J.; Xia, L. Distribution Forecast of Source Rocks and Gas Generation Potential of Shahezi Formation in Deep Fault Depressions of Songliao Basin. *Glob. Geol.* **2014**, *33*, 630–639, (In Chinese with English abstract).
59. Dong, Z. Sedimentary Environment and Organic Matter Enrichment of Shale in Upper Jiufotang, Ludong Sag, Kailu Basin. Master's Thesis, China University of Geosciences, Beijing, China, 2022; pp. 22–28, (In Chinese with English abstract).
60. Rong, H.; Jiao, Y.Q.; Wu, L.Q.; Wan, D.; Cui, Z.J.; Guo, X.J.; Jia, J.M. Origin of the Carbonaceous Debris and Its Implication for Mineralization within the Qianjiadian Uranium Deposit, Southern Songliao Basin. *Ore Geol. Rev.* **2019**, *107*, 336–352. [CrossRef]